energies

MDPI

Article

Resource Recovery and Synthesis of Battery-Grade $FePO_4$ from Waste $LiFePO_4$ Battery Slag

Puliang Li [1,2], Yang Wang [1,2], Liying Zhu [3], Kun Zhang [3], Weifang Liu [4,*], Tao Chen [1,2] and Kaiyu Liu [1,2,*]

[1] College of Chemistry and Chemical Engineering, Central South University, Changsha 410083, China; lpl79@163.com (P.L.); 242311110@cus.edu.cn (Y.W.); taochen4486@163.com (T.C.)
[2] Hunan Provincial Key Laboratory of Chemical Power Sources, College of Chemisty and Chemical Engineering, Central South University, Changsha 410083, China
[3] Beijing Institute of Spacecraft System Engineering, Beijing 100094, China; 15810534258@163.com (L.Z.); zhang_kun287@126.com (K.Z.)
[4] College of Chemistry and Chemical Engineering, Hunan University of Science & Technology, Xiangtan 410082, China
* Correspondence: 1060161@hnust.edu.cn (W.L.); kaiyuliu309@163.com (K.L.)

Abstract: The effective recovery of valuable materials from spent $LiFePO_4$ batteries is crucial for resource sustainability and environmental protection. This study investigates the recovery of phosphorus iron slag from waste $LiFePO_4$ batteries, focusing on dissolution and impurity removal processes to produce battery-grade iron phosphate. Using high-temperature-activated dissolution, followed by precipitation/dissolution for impurity removal, we optimize conditions to ensure high recovery rates (up to 98.8% for $FePO_4$ under optimized conditions) and product purity. Our findings demonstrate that the proposed method effectively transforms waste slag into valuable iron phosphate, significantly reducing raw material costs and contributing to sustainable battery recycling practices. The regenerated $LiFePO_4$ cathode exhibits excellent electrochemical performance, achieving a discharge capacity of 160.7 mAh g^{-1} at 0.1 C, which meets market standard levels. This research provides a solid foundation for enhancing resource utilization and advancing circular economy principles in the battery industry.

Keywords: lithium-ion batteries; resource recovery; $LiFePO_4$ cathode; recycling

check for updates

Received: 4 March 2025
Revised: 2 April 2025
Accepted: 2 April 2025
Published: 4 April 2025

Citation: Li, P.; Wang, Y.; Zhu, L.; Zhang, K.; Liu, W.; Chen, T.; Liu, K. Resource Recovery and Synthesis of Battery-Grade $FePO_4$ from Waste $LiFePO_4$ Battery Slag. *Energies* **2025**, *18*, 1829. https://doi.org/10.3390/en18071829

Copyright: © 2025 by the authors. Licensee MDPI, Basel, Switzerland. This article is an open access article distributed under the terms and conditions of the Creative Commons Attribution (CC BY) license (https://creativecommons.org/licenses/by/4.0/).

1. Introduction

In the context of the global energy transition, lithium batteries have garnered widespread attention as a crucial energy storage technology [1–4]. With the rapid development of renewable energy, lithium batteries play a vital role in electric vehicles, renewable energy storage, and portable electronic devices. Among these, lithium-ion batteries using $LiFePO_4$ cathode material have become particularly favored in the market due to their high safety, low cost, and long cycle life [5–8]. However, as early generations of $LiFePO_4$ batteries gradually reach the end of their service life, the effective recovery of their resources, especially battery-grade phosphoric acid iron, has emerged as an urgent challenge that needs to be addressed [9,10]. Thus, exploring new recovery methods and technologies is essential for achieving sustainable development [11–14].

Currently, the recycling of used batteries primarily focuses on the extraction of high-value metals such as lithium, while elements like phosphorus and iron are often overlooked [15–18]. For instance, conventional sulfuric acid leaching methods achieve Li recovery rates of 85–93% but require high acid consumption (2–3 g H_2SO_4/g Fe) and

fail to address $FePO_4$ utilization [5,19–21]. This neglect not only impacts the overall resource utilization rate but also poses significant environmental pollution risks [22–25]. Recent studies highlight alternative approaches: organic acids like citric acid (lemon juice) achieve 94.8% Li recovery with minimal Fe loss (<4%) [26], while formic acid systems enable selective Li extraction (95% efficiency) with 50% lower acid consumption than mineral acids [27]. The waste generated from $LiFePO_4$ batteries, particularly the iron phosphate slag, is typically regarded as a worthless byproduct [28,29]. However, this research advanced strategies such as high-temperature activation (800 °C) combined with precipitation/dissolution which have demonstrated $FePO_4$ recovery rates exceeding 98.8%, surpassing conventional hydrometallurgical methods. To achieve the recycling of battery materials, effective strategies must be developed to treat these wastes and transform them into valuable products [30–33]. Notably, regenerated $LiFePO_4$ from recycled $FePO_4$ exhibits competitive electrochemical performance (160.7 mAh g^{-1} at 0.1 C), comparable to commercial counterparts (155–170 mAh g^{-1}). This approach will not only enhance the comprehensive utilization of resources but also alleviate the pressure of waste disposal, thus promoting the development of a circular economy [26,34–36].

The core objective of this study is to explore the feasibility of using iron phosphate slag derived from the recycling of waste $LiFePO_4$ batteries as a raw material for the production of battery-grade phosphoric acid iron [37]. Through systematic experimental design, we will focus on investigating the dissolution and impurity removal processes of iron phosphate slag to optimize preparation conditions and ensure the quality of the final product [38,39]. Specifically, we will compare the effectiveness of different dissolution methods and explore suitable impurity removal techniques to enhance the purity and stability of phosphoric acid iron. This process will provide a solid technical foundation for the realization of waste resource reutilization.

Through this research, we aim to offer new insights and methods for the resource utilization of waste batteries, thereby promoting the achievement of sustainable development goals. Additionally, the findings will provide theoretical support for related enterprises in improving their technologies within the battery recycling sector, facilitating the circular economy of battery materials. Ultimately, we hope to contribute to the sustainable development of the industry and promote the green recycling and reuse technologies for battery materials on a broader scale.

2. Materials and Method

2.1. Material Recovery

The chemical reagents used and their specifications are shown in Table 1.

Table 1. Chemicals and specifications.

Chemical Name	Chemical Formula	Specifications
Ammonium Hydroxide	NH_4OH	28–30% solution
Phosphoric Acid	H_3PO_4	85% (concentrated)
Lithium Carbonate	Li_2CO_3	≥99% purity
Glucose	$C_6H_{12}O_6$	≥99% purity
Acetylene Black	C_8H_8	Conductive carbon black
Polyvinylidene Fluoride	PVDF	≥98% purity
Nitrogen	N_2	≥99.99% purity (for inert atmosphere)
Deionized Water	H_2O	Conductivity < 0.1 μS/cm
Aqua Regia	N/A	HNO_3:HCl (3:1 v/v) for analysis

2.1.1. Dissolution of Iron Phosphate Residue

The iron phosphate slag in this study, derived from recycled lithium-ion batteries, primarily consists of iron phosphate and carbon, along with a significant amount of impurities. Two dissolution methods were employed: first, a direct dissolution method, where the waste iron phosphate was added to a solution of sulfuric acid at a specific concentration (6–8 M) and stirred for a designated period (4–6 h) to facilitate dissolution. Second, the iron phosphate slag was first subjected to high-temperature sintering in a muffle furnace, after which the waste iron phosphate was added to a solution of sulfuric acid at the same concentration (6–8 M) and stirred for a designated period (3–4 h) to achieve dissolution. All dissolution steps were performed under ambient atmospheric conditions, and the dissolution temperature was maintained at 60–70 °C.

2.1.2. Impurity Removal

A certain amount of a purification agent was added to the leachate to prevent aluminum from precipitating. Ammonium hydroxide was used to adjust the pH of the leachate to approximately 2. Under these conditions, the purification agent allows aluminum to remain in solution, while iron phosphate precipitates first. After solid–liquid separation, sulfuric acid is added to dissolve the precipitated iron phosphate, resulting in a qualified purification solution.

2.1.3. Regeneration of Iron Phosphate

The purified ferrous phosphate slag solution was placed in a flask, to which an equal volume of water was added. Under constant stirring at a temperature of 40 °C, ammonium hydroxide was introduced into the solution to adjust the pH to 2.2–2.5. The concentration of iron phosphate in the solution was monitored to ensure optimal conditions for precipitation. The solution was then filtered and washed until the conductivity was below 500 μS/cm, indicating the removal of impurities. The resulting filter cake was collected, and pure water was added, followed by phosphoric acid, ensuring thorough mixing. The slurry was then poured into a flask and aged by stirring for 3 h at 92 °C. After aging, the slurry was filtered and washed until the conductivity was below 200 μS/cm. The filter cake was subsequently dried at 105 °C for 12 h to obtain dihydrate iron phosphate. This dihydrate iron phosphate was placed in a ceramic crucible and sintered in a muffle furnace at a temperature of 560 °C for 4 h to yield the recovered anhydrous iron phosphate.

2.1.4. Synthesis of $LiFePO_4$

Using the previously prepared iron phosphate precursor as the raw material, lithium carbonate and glucose were added in specific proportions (with a Li/Fe ratio of 1.05 and glucose constituting 10% of the total mass of lithium carbonate and iron phosphate). The solid content was controlled at 45%. The mixture was then milled in pure water until the D50 value of the particle size distribution reached 0.35–0.4 μm, determined using laser diffraction particle size analysis (Malvern Mastersizer 3000), resulting in a precursor mixture. This slurry was spray-dried to obtain a fully dried precursor. Subsequently, the dried precursor was placed in a quartz crucible and subjected to sintering in a tubular furnace under a nitrogen atmosphere at a temperature of 740 °C for 8 h, producing $LiFePO_4$ cathode material.

2.2. Material Characterization

X-ray diffraction patterns were acquired using a Bruker Advance-D8 diffractometer, employing Cu Kα radiation as the source. The cell parameters were refined using GSAS software (version 2.0) following the Rietveld method. Solid samples (such as phosphorous

iron slag) were digested using a mixed acid solution of HNO_3 and HCl (aqua regia, 3:1 v/v) at 120 °C for 2 h. The solution was then filtered and diluted with deionized water, followed by elemental analysis via inductively coupled plasma optical emission spectrometry (ICP-OES, PerkinElmer Avio 500). Additionally, the morphologies of the materials were observed through scanning electron microscopy (SEM) images, utilizing a FEI Nova Nano SEM 230 instrument.

2.3. Electrochemical Test

To investigate the electrochemical properties of the fabricated cathode materials, coin-type (CR2016) cells were assembled in an argon-filled glove box. The electrode was prepared by combining the active material, acetylene black, and polyvinylidene fluoride (PVDF) in a weight ratio of 8:1:1 onto aluminum foils, using N-methyl-2-pyrrolidone (NMP) as the solvent. The prepared electrodes were then dried in a vacuum oven at 80 °C for 24 h. The mass loading of the active materials ranged from 1.5 to 2 mg/cm^2. Charge and discharge measurements were conducted using the NEWARE battery test system.

3. Results and Discussion

3.1. Dissolution of Iron Phosphate Slag

3.1.1. Direct Dissolution Method

According to the literature, elevated temperatures (>70 °C) and extended dissolution durations (>6 h) promote the precipitation of $FePO_4$, which may react to form abnormal phosphoric acid iron, adversely affecting its dissolution efficiency [27]. The optimal dissolution rate occurs at temperatures between 60 and 70 °C. At this temperature and under high acidity, dissolving for 4–6 h minimizes the precipitation of dissolved iron and phosphorus. Therefore, the chosen dissolution temperature was 60–70 °C, with a dissolution time set at 4–6 h.

Experiments were conducted under the same dissolution conditions using the direct dissolution method. After completion, the mixture was filtered, and the volumes of the filtrate and weights of the residue were recorded. The iron content in both the filtrate and residue was measured, with the recovery rate calculated using the following Formula (1):

$$\text{Recovery Rate} = (\text{Filtrate iron concentration} \times \text{Filtrate volume})/(\text{Filtrate iron concentration} \times \text{Filtrate volume} + \text{Residue iron content} \times \text{Residue weight}) \times 100 \quad (1)$$

Table 2 below presents the recovery rates from the direct dissolution method, calculated based on iron (notably, the recovery rate for phosphorus is higher than that for iron).

Table 2. Recovery data for direct dissolution method.

Test Group	Amount of Iron Phosphate Slag (g)	Amount of Acid Added (g)	Sulfuric per g of Iron	Recovery Rate
Group 1	1000	500 g sulfuric acid	2.43	83.3%
Group 2	1000	600 g sulfuric acid	2.92	40.19%
Group 3	1000	700 g sulfuric acid	3.4	39.82%
Group 4	1000	800 g sulfuric acid	3.89	78.48%

This approach primarily validates the effects of 500 g, 600 g, 700 g, and 800 g sulfuric acid on the dissolution of iron phosphate slag. Higher quantities of sulfuric acid were not included in the experimental plan, as the acidity of the resulting leachate is closely related to the amount of sulfuric acid added. While increasing sulfuric acid might enhance recovery rates, excessive acidity would adversely affect subsequent reactions in phosphoric acid iron synthesis.

From the data presented in the table, it is evident that the overall recovery rate for iron phosphate slag is not high and exhibits instability, with a maximum of 83.3% and a minimum of only 39.82%. The low recovery rate may be related to the properties of the iron phosphate slag, where iron and phosphorus primarily exist as precipitated phosphoric acid iron and may have formed dihydrate phosphoric acid iron, leading to lower recovery rates. The instability in recovery rates could also stem from the raw materials, as different manufacturers may have varying processes for recovering iron phosphate slag, resulting in differing amounts of dihydrate phosphoric acid iron and ultimately unstable recovery rates.

An isolated analysis of the impact of sulfuric acid addition on the recovery filtrate did not reveal a consistent trend of increased recovery with greater sulfuric acid amounts. This suggests that the soluble portion of iron phosphate in the slag does not require substantial sulfuric acid, and the remaining insoluble components are difficult to dissolve even with increased acidity.

3.1.2. High-Temperature-Activated Dissolution Method

In this experimental approach, iron phosphate slag was first high-temperature-sintered in a muffle furnace before undergoing dissolution at a temperature of 60–70 °C for 3–4 h. Table 3 below presents the recovery rate data for the high-temperature-activated dissolution method.

Table 3. Recovery data for high-temperature activation method.

Activation Temperature	Group	Amount of Iron Phosphate Slag (g)	Amount of Acid Added (g)	Sulfuric Acid per g of Iron	Recovery Rate
500 °C	Group T1	1000	875	2.5	79.28%
	Group T2	1000	800	2.26	93.86%
560 °C	Group T3	1000	800	2.26	91.89%
	Group T4	1000	800	2.26	86.26%
	Group T5	1000	600	1.7	90.43%
	Group T6	1000	600	1.7	87.64%
	Group T7	1000	600	1.7	93.14%
	Group T8	1000	600	1.7	87.50%
800 °C	Group T9	1000	300	0.85	57.23%
	Group T10	1000	400	1.13	91.04%
	Group T11	1000	430	1.22	93.35%
	Group T12	1000	440	1.25	98.80%
	Group T13	1000	450	1.27	96.48%
	Group T13	1000	450	1.27	92.92%

The purpose of high-temperature activation is to ensure that all phosphoric acid iron in the iron phosphate slag exists in the form of anhydrous phosphoric acid iron. Unlike the dehydration process of phosphoric acid, the focus here is solely on the effect of activation temperature, with a constant activation time of 3 h.

During the high-temperature activation process, a visible transformation occurred in the appearance of the iron phosphate slag. The unactivated slag appeared as a black solid powder, while the slag activated at 500 °C and 560 °C exhibited a yellow-white surface, although agglomeration occurred during activation, with the interior remaining black. The slag activated at 800 °C turned entirely yellow-white, indicating a significant impact of activation temperature on the activation process.

The following discussion examines the influence of activation temperature on the dissolution of iron phosphate slag. Overall, high-temperature activation is beneficial for improving the recovery rate of iron phosphate slag compared to the direct dissolution

method, as shown in Figure 1. Under sufficient sulfuric acid conditions, the recovery rate can be maintained above 80%.

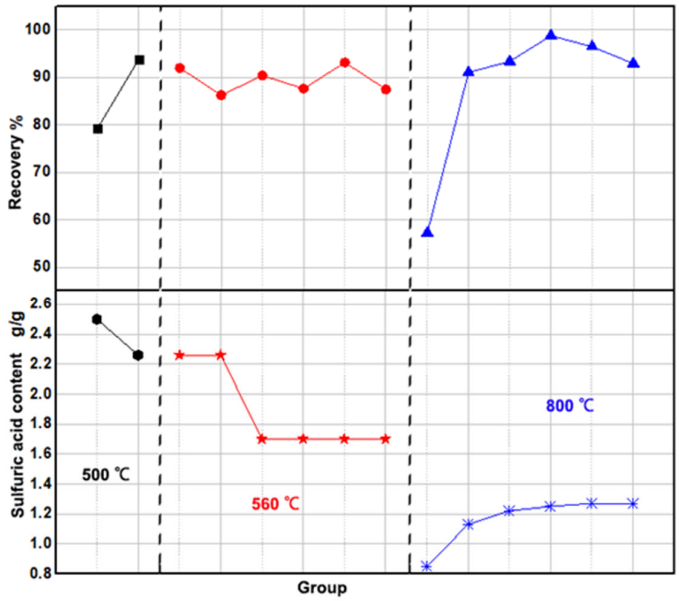


Figure 1. Effect of activation temperature and amount of dissolved sulfuric acid on recovery.

At an activation temperature of 500 °C, the recovery rate exceeded 80%. However, in this case, experiments with higher sulfuric acid quantities did not yield higher recovery rates than those with lower quantities. For instance, the recovery rate with higher sulfuric acid was 79.28%, while that with lower acid reached 93.86%. This inconsistency may result from the incomplete activation of the slag at 500 °C, leading to uneven distribution within the material and, consequently, unstable recovery rates.

Raising the temperature to 560 °C stabilized recovery above 85%, peaking at 93.14% with reduced sulfuric acid. At 800 °C, recovery exceeded 90%, reaching 98.8%, while acid use dropped by about 50%. However, excessively high temperatures may volatilize phosphorus and convert iron to ferric oxide, making 800 °C the optimal choice. The amount of sulfuric acid also plays a critical role in recovery. The study found that a peak recovery of 98.8% occurred at 1.25 g sulfuric acid, with the optimal range for effective recovery being 1.22 to 1.27 g.

In summary, the high-temperature-activated dissolution method achieves over 90% recovery, presenting a more efficient alternative to direct dissolution with roughly 50% less sulfuric acid. The ideal conditions for optimal recovery are an activation temperature of 800 °C, 1.27 g sulfuric acid per gram of iron, a dissolution temperature of 60–70 °C, and a dissolution time of 3–4 h.

3.2. Impurity Removal from Solution

The filtrate of Group 12 obtained from the dissolution of phosphorus iron slag showed impurity contents as presented in Table 4. The main impurities were aluminum (Al) and titanium (Ti), with Al exceeding 300 ppm and Ti exceeding 150 ppm, while other impurities were relatively low. The Al originates from the battery current collectors, and Ti comes from the doping of lithium iron. Both Al and Ti exist in the form of metal salts. If Al and Ti are not removed and phosphorus iron is synthesized directly, these impurities will contaminate the product, resulting in excessive levels of Al and Ti. Currently, the manufacturing of $LiFePO_4$ typically incorporates Ti during production; therefore, it may be feasible to retain the Ti element while removing Al.

Table 4. Impurity content of phosphorus iron slag after dissolution in Group 12.

Group	Element Content (ppm)													
	Al	**Ca**	**Cd**	**Co**	**Cr**	**Cu**	**Mg**	**Mn**	**Na**	**Ni**	**K**	**Pb**	**Ti**	**Zn**
Group 12	323.1	5.331	0.09	2.882	3.861	0.968	5.111	12.29	106.1	11.78	5.011	3.33	149.6	1.244

For the impurity removal process, we employed a precipitation/dissolution method. First, the removing agent was dissolved in the leachate, and then ammonia was diluted tenfold. The diluted ammonia was added to the leachate, adjusting the pH to 2, followed by stirring for 30 min. The mixture was then filtered, and the filter cake was mixed with pure water and sulfuric acid to ensure the complete dissolution of the precipitate. As shown in Figure 2, the addition of ammonium fluoride to the leachate effectively removed aluminum, and within a certain range, the aluminum removal efficiency increased with the amount of ammonium fluoride added. Without ammonium fluoride, the aluminum removal efficiency was 88.99%. With the addition of 0.025 g/L of ammonium fluoride, the aluminum removal rate increased to 92.37%. When the ammonium fluoride concentration was increased to 0.1 g/L, the aluminum removal rate reached 97.42%. However, further increasing the ammonium fluoride amount to 0.2 g/L resulted in a slight decrease in aluminum removal efficiency to 97.11%. Therefore, the optimal amount of the removing agent was determined to be 0.1 g/L.

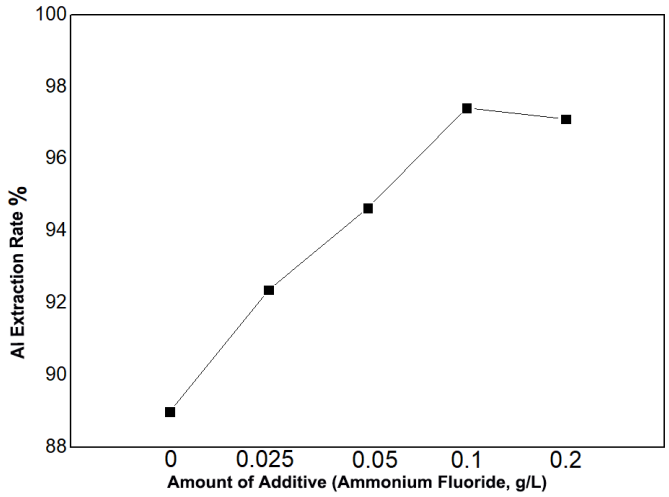


Figure 2. Effect of ammonium fluoride addition on aluminum removal efficiency.

3.3. Regeneration for the Preparation of Battery-Grade Iron Phosphate

Using the purified filtrate, recovered iron phosphate was prepared. The synthesized iron phosphate is shown in Figure 3. The XRD patterns indicate sharp diffraction peaks and distinct characteristic peaks, indicating the high crystallinity of the sample. Comparison with standard cards revealed that the sample pattern was consistent with the standard card for iron phosphate (29-0715), with no additional peaks, suggesting the high purity of the sample. In the SEM results of the synthesized $FePO_4$ (Figure 4), the particles were observed to be uniformly dispersed, with a diameter of approximately 100 nm. This uniform dispersion is crucial for the subsequent synthesis of $LiFePO_4$. The smaller particle size not only increases the reaction surface area but also enhances the contact between reactants, facilitating a more complete reaction. The fine $FePO_4$ particles are likely to interact more effectively with the lithium source, potentially leading to a more efficient synthesis process for $LiFePO_4$ and improved electrochemical performance. These findings

underscore the importance of optimizing particle size and distribution for achieving high-quality $LiFePO_4$ synthesis.

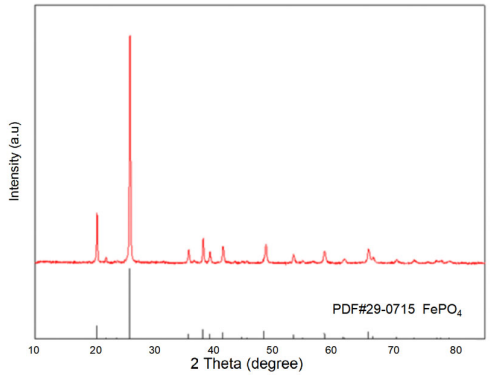


Figure 3. The XRD pattern of $FePO_4$ prepared under optimized conditions for Group 12.

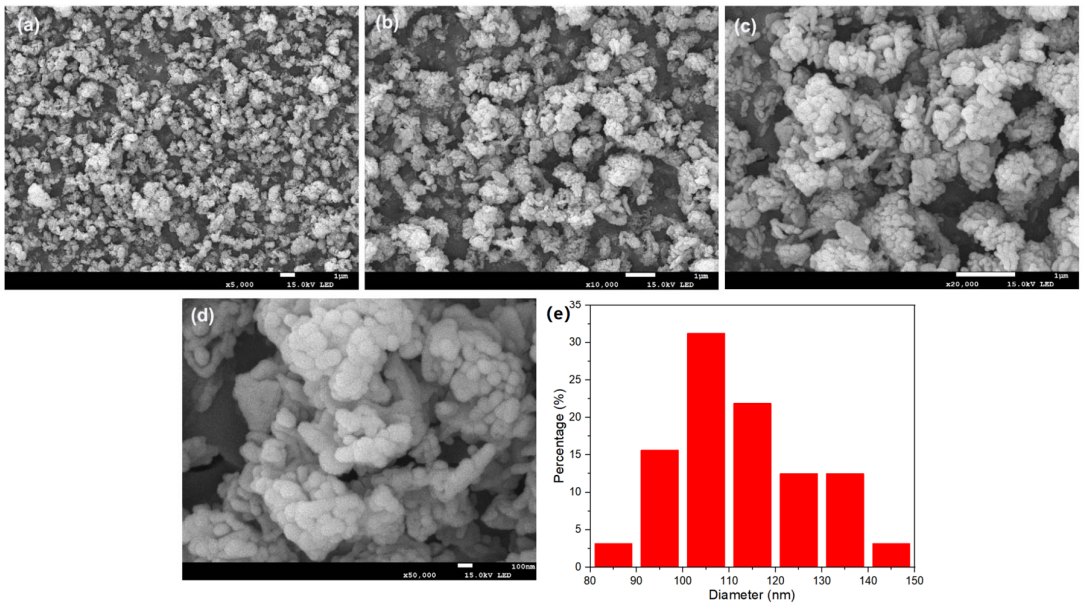


Figure 4. (**a**–**d**) SEM images of the as-prepared $FePO_4$ at different magnifications; (**e**) particle size distribution histogram of $FePO_4$.

3.4. Regeneration of $LiFePO_4$

Using the previously prepared iron phosphate precursor as the raw material, $LiFePO_4$ cathode material was regenerated. The images of the obtained $LiFePO_4$ are shown in Figure 5. It can be observed that the prepared $LiFePO_4$ cathode material exhibited a relatively uniform distribution with overall good dispersion, showing only slight agglomeration. Additionally, as shown in the charge and discharge curves in Figure 6, the regenerated $LiFePO_4$ exhibited a discharge capacity of 160.7 mAh g^{-1}, with a coulombic efficiency of 99%. This performance is nearly comparable to that of commercially available $LiFePO_4$. Furthermore, measurements of the tap density revealed a value of 2.45 g cm^{-3}. These results indicate that $LiFePO_4$ synthesized from recycled iron phosphate has promising application potential.

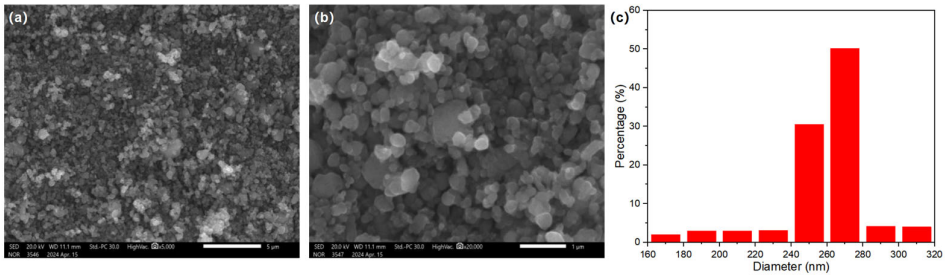


Figure 5. (**a**,**b**) SEM images of $LiFeO_4$ at different magnifications; (**c**) particle size distribution histogram of LiFePO4.

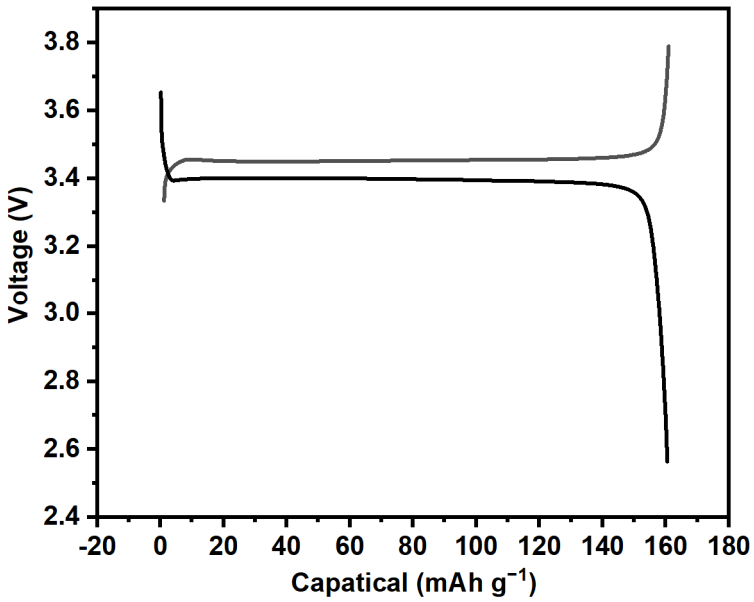


Figure 6. Charge and discharge curves of the as-prepared $LiFePO_4$ at a current density of 0.1 C.

As shown in Figure 7a, the prepared $LiFePO_4$ exhibited a reversible discharge capacity of 150 mAh g^{-1} at a current density of 1 C. After 145 cycles, it retained 92.75% of its initial capacity. Additionally, at 2 C, the initial specific capacity was 127.85 mAh g^{-1}, and after 160 cycles, the capacity faded by only 9.56%, as shown in Figure 7b. Furthermore, its reversible specific capacities at 0.1 C, 0.2 C, 0.5 C, 1 C, and 2 C were 164.07, 162.33, 155.92, 149.88, and 134.77 mAh g^{-1}, respectively (Figure 7c). According to the CV results (Figure 7d), the discharge plateau was at 3.4 V, and the charge plateau was just below 3.5 V, maintaining a small overpotential, which was consistent with the charge/discharge curves. The EIS results (Figure 8) showed that the internal resistance of the battery was only about 58 ohms, indicating excellent kinetics due to its relatively low internal resistance. Additionally, the Solution Resistance (R_{SC}) was extracted from the high-frequency intercept (>10^4 Hz) on the real axis, with a fitted value of R_{SC} = 5.2 Ω. This indicates low ohmic resistance due to the high ionic conductivity of the electrolyte and good electrode-electrolyte contact. The Charge Transfer Resistance (R_{CT}) was determined from the diameter of the semicircle in the mid-frequency range (10^2–10^0 Hz), yielding a fitted value of R_{CT} = 52.8 Ω. This reflects efficient charge transfer kinetics at the electrode/electrolyte interface, which is critical for fast Li^+ intercalation/deintercalation. Furthermore, the Warburg Impedance (W_0), represented by the linear slope in the low-frequency region (<10^{-1} Hz), is associated with solid-state Li^+ diffusion; a near-45° slope confirms diffusion-dominated behavior.

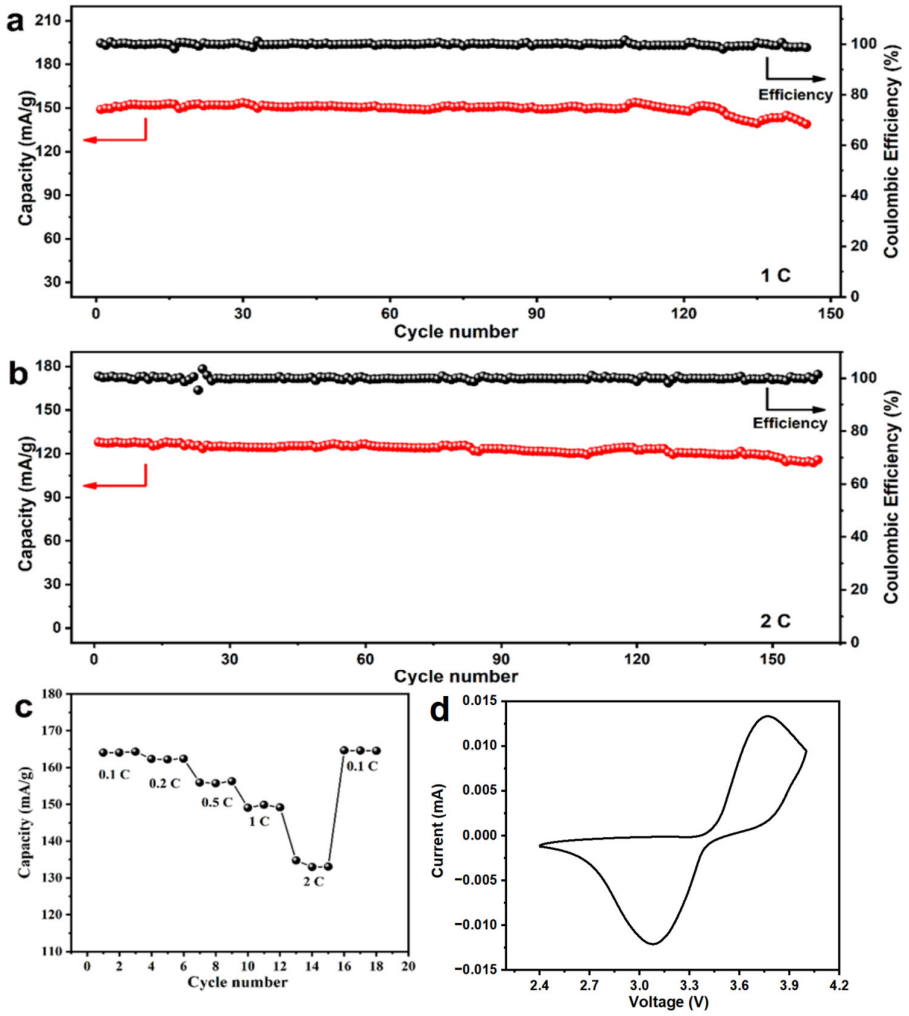


Figure 7. Electrochemical performance of prepared $LiFePO_4$ at (**a**) 1 C; (**b**) 2 C; (**c**) different rates and (**d**) CV curve.

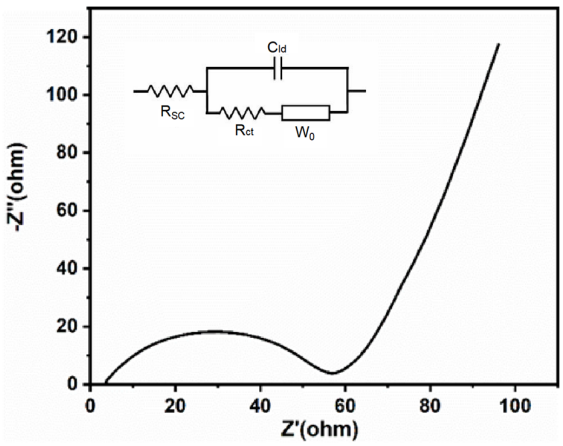


Figure 8. EIS curve and equivalent circuit model of recovered $LiFePO_4$.

4. Conclusions

This study used waste phosphorus iron slag from the recycling of old $LiFePO_4$ batteries as raw material to investigate the recovery and dissolution conditions of phosphorus iron slag, as well as impurity removal methods. It also explored the process conditions for synthesizing battery-grade iron phosphate from the leachate of phosphorus iron slag. Moreover, the $LiFePO_4$ cathode material produced from the reaction of iron phosphate

waste residue with lithium carbonate reached the performance level of mainstream $LiFePO_4$ cathode materials in the market, demonstrating excellent electrochemical properties. In summary, utilizing phosphorus iron slag as the raw material, employing high-temperature-activated dissolution followed by precipitation/dissolution for impurity removal, and synthesizing battery-grade iron phosphate from the treated leachate is a viable route. This method facilitates the resource utilization of waste phosphorus iron slag from old $LiFePO_4$ batteries, reduces raw material costs, and holds significant practical implications.

Author Contributions: Conceptualization, P.L.; Methodology, P.L.; Software, P.L.; Validation, P.L.; Formal analysis, P.L.; Data curation, P.L.; Writing—original draft, P.L.; Writing—review and editing, Y.W., T.C. and K.Z.; Visualization, P.L., K.L. and L.Z.; Supervision, W.L. and K.L.; Project administration, L.Z., T.C. and K.L. All authors have read and agreed to the published version of the manuscript.

Funding: This research was funded by the National Natural Science Foundation of China (No. 22272204), the Hunan Provincial Natural Science Foundation Project (No.2023JJ40276), and the Beijing Nova Program (No. 20220484153).

Data Availability Statement: The original contributions presented in the study are included in the article, and further inquiries can be directed to the corresponding author.

Conflicts of Interest: The authors declare no conflicts of interest.

References

1. Kumar, J.; Neiber, R.R.; Park, J.; Ali Soomro, R.; Greene, G.W.; Ali Mazari, S.; Young Seo, H.; Hong Lee, J.; Shon, M.; Wook Chang, D.; et al. Recent progress in sustainable recycling of $LiFePO_4$-type lithium-ion batteries: Strategies for highly selective lithium recovery. *Chem. Eng. J.* **2022**, *431*, 133993–134008. [CrossRef]
2. Chen, T.; Qiu, C.; Zhang, X.; Wang, H.; Song, J.; Zhang, K.; Yang, T.; Zuo, Y.; Yang, Y.; Gao, C.; et al. An Ultrasmall Ordered High-Entropy Intermetallic with Multiple Active Sites for the Oxygen Reduction Reaction. *J. Am. Chem. Soc.* **2024**, *146*, 1174–1184. [CrossRef] [PubMed]
3. Peng, C.; Liang, S.; Yu, Y.; Cao, L.; Yang, C.; Liu, X.; Guo, K.; Müller-Buschbaum, P.; Cheng, Y.J.; Wang, C. A chronicle of titanium niobium oxide materials for high-performance lithium-ion batteries: From laboratory to industry. *Carbon Neutralization* **2024**, *3*, 1036–1091. [CrossRef]
4. Han, Y.; Zhou, X.; Fang, R.; Lu, C.; Wang, K.; Gan, Y.; He, X.; Zhang, J.; Huang, H.; Zhang, W.; et al. Supercritical carbon dioxide technology in synthesis, modification, and recycling of battery materials. *Carbon Neutralization* **2023**, *2*, 169–185. [CrossRef]
5. Zheng, R.; Zhao, L.; Wang, W.; Liu, Y.; Ma, Q.; Mu, D.; Li, R.; Dai, C. Optimized Li and Fe recovery from spent lithium-ion batteries via a solution-precipitation method. *RSC Adv.* **2016**, *6*, 43613–43625. [CrossRef]
6. Yin, R.-X.; Zhu, W.-G.; Zhao, Z.-W.; Xu, W.-H.; Liu, X.-H.; He, L.-H. Lithium recovery from brine by PEG-modified porous $LiFePO_4/FePO_4$ electrode system. *Sep. Purif. Technol.* **2024**, *338*, 126375–126383. [CrossRef]
7. Du, H.; Kang, Y.; Li, C.; Zhao, Y.; Tian, Y.; Lu, J.; Chen, Z.; Gao, N.; Li, Z.; Wozny, J.; et al. Recovery of lithium salt from spent lithium-ion battery by less polar solvent wash and water extraction. *Carbon Neutralization* **2023**, *2*, 416–424. [CrossRef]
8. Ren, J.; Zhu, H.; Fang, Y.; Li, W.; Lan, S.; Wei, S.; Yin, Z.; Tang, Y.; Ren, Y.; Liu, Q. Typical cathode materials for lithium-ion and sodium-ion batteries: From structural design to performance optimization. *Carbon Neutralization* **2023**, *2*, 339–377. [CrossRef]
9. Hu, G.; Huang, K.; Du, K.; Peng, Z.; Cao, Y. Efficient recovery and regeneration of $FePO_4$ from lithium extraction slag: Towards sustainable $LiFePO_4$ battery recycling. *J. Clean. Prod.* **2024**, *434*, 140091–140101. [CrossRef]
10. Bai, L.; Liu, G.; Fu, Y.; Sun, W.; Zeng, X.; Shao, R.; Ou, H.; Liang, Y.; Yuan, F. Approach towards the Purification Process of $FePO_4$ Recovered from Waste Lithium-Ion Batteries. *Processes* **2024**, *12*, 1861. [CrossRef]
11. Wang, Y.; Cao, G. Developments in Nanostructured Cathode Materials for High-Performance Lithium-Ion Batteries. *Adv. Mater.* **2008**, *20*, 2251–2269. [CrossRef]
12. Wang, X.; Gaustad, G.; Babbitt, C.W.; Richa, K. Economies of scale for future lithium-ion battery recycling infrastructure. *Resour. Conserv. Recycl.* **2014**, *83*, 53–62. [CrossRef]
13. Scrosati, B.; Garche, J. Lithium batteries: Status, prospects and future. *J. Power Sources* **2010**, *195*, 2419–2430. [CrossRef]
14. Chen, T.; Cai, J.; Wang, H.; Gao, C.; Yuan, C.; Zhang, K.; Yu, Y.; Xiao, W.; Luo, T.; Xia, D. Symbiotic reactions over a high-entropy alloy catalyst enable ultrahigh-voltage Li–CO_2 batteries. *Energy Environ. Sci.* **2025**, *18*, 853–861. [CrossRef]
15. Gören, A.; Costa, C.M.; Silva, M.M.; Lanceros-Mendez, S. Influence of fluoropolymer binders on the electrochemical performance of C-$LiFePO_4$ based cathodes. *Solid State Ion.* **2016**, *295*, 57–64. [CrossRef]

16. Yang, S.; Song, Y.; Ngala, K.; Zavalij, P.Y.; Stanley Whittingham, M. Performance of $LiFePO_4$ as lithium battery cathode and comparison with manganese and vanadium oxides. *J. Power Sources* **2003**, *119–121*, 239–246. [CrossRef]
17. Kakarla, A.K.; Narsimulu, D.; Bandi, H.; Shanthappa, R.; Yu, J.S. Facile synthesis of N-doped reduced graphene oxide matrix-covered porous Fe_2VO_4 hybrid composite nanostructures as anode material for lithium-ion batteries. *J. Alloys Compd.* **2023**, *960*, 170784. [CrossRef]
18. Kakarla, A.K.; Narsimulu, D.; Patnam, H.R.; Shanthappa, R.; Yu, J.S. Structural and electrochemical properties of mesoporous $FeVO_4$ as a negative electrode for lithium-ion battery. *Int. J. Energy Res.* **2022**, *46*, 13590–13601. [CrossRef]
19. Zhang, Y.; Ru, J.; Hua, Y.; Cheng, M.; Lu, L.; Wang, D. Priority Recovery of Lithium From Spent Lithium Iron Phosphate Batteries via H_2O-Based Deep Eutectic Solvents. *Carbon Neutralization* **2025**, *4*, e186. [CrossRef]
20. Tang, R.; Dong, J.; Wang, C.; Yin, A.; Lu, Y.; Li, N.; Shen, W.; Zhang, J.; Yan, K.; Zhao, G.; et al. A Comprehensive Review of the Research Progress on the Low-Temperature Performance of $LiFePO_4$ Batteries. *Carbon Neutralization* **2025**, *4*, e70001. [CrossRef]
21. Zhou, Y.; Pang, M.; Zhang, M.; Yuan, Y.; Yang, Y.; Qin, F.; Liu, W.; Chen, T.; Liu, K. Controlling crystallographic orientation through composite phase regulation to unlock oxide cathode performance. *Chem. Eng. J.* **2024**, *501*, 157527. [CrossRef]
22. Nigl, T.; Schwarz, T.E.; Walch, C.; Baldauf, M.; Rutrecht, B.; Pomberger, R. Characterisation and material flow analysis of end-of-life portable batteries and lithium-based batteries in different waste streams in Austria. *Waste Manag. Res.* **2020**, *38*, 649–659. [CrossRef] [PubMed]
23. Cai, G.; Fung, K.Y.; Ng, K.M.; Wibowo, C. Process Development for the Recycle of Spent Lithium Ion Batteries by Chemical Precipitation. *Ind. Eng. Chem. Res.* **2014**, *53*, 18245–18259. [CrossRef]
24. Li, X.; Zhang, J.; Song, D.; Song, J.; Zhang, L. Direct regeneration of recycled cathode material mixture from scrapped $LiFePO_4$ batteries. *J. Power Sources* **2017**, *345*, 78–84. [CrossRef]
25. Chen, T.; Ouyang, B.; Fan, X.; Zhou, W.; Liu, W.; Liu, K. Oxide cathodes for sodium-ion batteries: Designs, challenges, and perspectives. *Carbon Energ.* **2022**, *4*, 170–199. [CrossRef]
26. Kumar, J.; Shen, X.; Li, B.; Liu, H.; Zhao, J. Selective recovery of Li and $FePO_4$ from spent $LiFePO_4$ cathode scraps by organic acids and the properties of the regenerated $LiFePO_4$. *Waste Manag. Res.* **2020**, *113*, 32–40. [CrossRef]
27. Ali, M.; Iqbal, N.; Noor, T.; Zaman, N. Selective lithium recovery from spent LFP Li-ion batteries using organic acids. *Ionics* **2024**, *31*, 273–286. [CrossRef]
28. Huang, B.; Pan, Z.; Su, X.; An, L. Recycling of lithium-ion batteries: Recent advances and perspectives. *J. Power Sources* **2018**, *399*, 274–286. [CrossRef]
29. Gao, R.; Xu, Z. Pyrolysis and utilization of nonmetal materials in waste printed circuit boards: Debromination pyrolysis, temperature-controlled condensation, and synthesis of oil-based resin. *J. Hazard. Mater.* **2019**, *364*, 1–10. [CrossRef]
30. Wang, L.; Li, J.; Zhou, H.; Huang, Z.; Tao, S.; Zhai, B.; Liu, L.; Hu, L. Regeneration cathode material mixture from spent lithium iron phosphate batteries. *J Mater. Sci.-Mater. Electron.* **2018**, *29*, 9283–9290. [CrossRef]
31. Jung, J.C.-Y.; Sui, P.-C.; Zhang, J. A review of recycling spent lithium-ion battery cathode materials using hydrometallurgical treatments. *J. Energy Storage* **2021**, *35*, 102217–102237. [CrossRef]
32. Diekmann, J.; Hanisch, C.; Froböse, L.; Schälicke, G.; Loellhoeffel, T.; Fölster, A.-S.; Kwade, A. Ecological Recycling of Lithium-Ion Batteries from Electric Vehicles with Focus on Mechanical Processes. *J. Electrochem. Soc.* **2016**, *164*, A6184–A6191. [CrossRef]
33. Li, L.; Bian, Y.; Zhang, X.; Yao, Y.; Xue, Q.; Fan, E.; Wu, F.; Chen, R. A green and effective room-temperature recycling process of $LiFePO_4$ cathode materials for lithium-ion batteries. *Waste Manag. Res.* **2019**, *85*, 437–444. [CrossRef] [PubMed]
34. Hanisch, C.; Loellhoeffel, T.; Diekmann, J.; Markley, K.J.; Haselrieder, W.; Kwade, A. Recycling of lithium-ion batteries: A novel method to separate coating and foil of electrodes. *J. Clean. Prod.* **2015**, *108*, 301–311. [CrossRef]
35. Zhong, X.; Liu, W.; Han, J.; Jiao, F.; Qin, W.; Liu, T.; Zhao, C. Pyrolysis and physical separation for the recovery of spent $LiFePO_4$ batteries. *Waste Manag. Res.* **2019**, *89*, 83–93. [CrossRef]
36. Pan, M.; Wang, Y.; Liu, Y.; Zhang, M.; Liu, X.; Yuan, Y.; Zhou, Y.; Liu, W.; Chen, T.; Liu, K. Optimizing interfacial modification for enhanced performance of $Na_3V_2(PO_4)_3$ cathode in sodium-ion batteries. *Chem. Eng. J.* **2024**, *495*, 153396. [CrossRef]
37. Ku, H.; Jung, Y.; Jo, M.; Park, S.; Kim, S.; Yang, D.; Rhee, K.; An, E.M.; Sohn, J.; Kwon, K. Recycling of spent lithium-ion battery cathode materials by ammoniacal leaching. *J. Hazard. Mater.* **2016**, *313*, 138–146. [CrossRef]
38. Zeng, X.; Li, J. Innovative application of ionic liquid to separate Al and cathode materials from spent high-power lithium-ion batteries. *J. Hazard. Mater.* **2014**, *271*, 50–56. [CrossRef]
39. Chen, D.; Rao, S.; Wang, D.; Cao, H.; Xie, W.; Liu, Z. Synergistic leaching of valuable metals from spent Li-ion batteries using sulfuric acid- l-ascorbic acid system. *Chem. Eng. J.* **2020**, *388*, 124321. [CrossRef]

Disclaimer/Publisher's Note: The statements, opinions and data contained in all publications are solely those of the individual author(s) and contributor(s) and not of MDPI and/or the editor(s). MDPI and/or the editor(s) disclaim responsibility for any injury to people or property resulting from any ideas, methods, instructions or products referred to in the content.